Article **Journal of Computational Technologies**
June, 2023 Vol.7 No.19 29-36

Preliminary study of thermography applied to diagnosed faults in Diesel Engine and network rack

Estudio preliminar de termografía aplicada en fallas diagnosticadas en Motor a Diesel y rack de redes

CARDENAS-SANCHEZ, Enrique†*, DELGADILLO-PARTIDA, Jorge, RAMOS-PONCE, Manuel and RIOS-HERNANDEZ, Juan

Ingeniería en Mantenimiento Industrial, Universidad tecnológica de Manzanillo

ID 1st Author: *Enrique, Cárdenas-Sánchez* / **ORC ID:** 0000-0001-7682-7213

ID 1st Co-author: *Jorge, Delgadillo-Partida* / **ORC ID:** 0000-0002-5078-008X

ID 2nd Co-author: *Manuel, Ramos-Ponce* / **ORC ID:** 0009-0008-4118-5079

ID 3rd Co-author: *Juan, Ríos-Hernández* / **ORC ID:** 0009-0002-6921-0869

DOI: 10.35429/JOCT.2023.19.7.29.36 Received March 15, 2023; Accepted June 28, 2023

Abstract

In this study, we applied thermographic analysis to gather data and establish decision criteria for the corrective maintenance of electrical and mechanical systems. Our main objective is to generate a thermographic database for systems such as combustion engines and network racks. To achieve this, we conducted preliminary experiments on electrical and mechanical systems with known faults. We also established calibration criteria for the thermal emissivity of the components. Subsequently, we analyzed a Diesel engine with induced faults, obtaining the maximum temperature threshold in malfunctioning components, as well as emissivity values. Additionally, we carried out an analysis on a network rack, specifically a 48-node Patch, with constant and intermittent connection faults. Our methodology included analyzing the transience of the mentioned systems to identify patterns indicating wear, malfunction, or damage. The collected data allowed us to create a database and perform calibration for effective emissivity.

Thermography, Corrective, Network, Dataset, Analysis

Resumen

En este estudio, aplicamos el análisis termográfico para recopilar datos y establecer criterios de decisión para el mantenimiento correctivo de sistemas eléctricos y mecánicos. Nuestro objetivo principal es generar una base de datos termográficos de sistemas, tales como motores de combustión y rack de redes. Para esto, realizamos experimentos previos en sistemas eléctricos y mecánicos con fallas conocidas. También establecimos criterios de calibración para la emisividad térmica de los componentes. Posteriormente, analizamos un motor a Diesel con fallas inducidas, obteniendo el umbral máximo de temperatura en componentes en mal funcionamiento, así como los valores de emisividad. Además, llevamos a cabo un análisis en un rack de redes, específicamente un Patch de 48 nodos, con fallas constantes e intermitentes de conexión. Nuestra metodología, incluyó el análisis de la transitoriedad de los sistemas mencionados para identificar patrones que indiquen desgaste, mal funcionamiento o daño. Los datos recopilados nos permitieron crear una base de datos, así como realizar una calibración para la emisividad efectiva.

Termografía, Base de datos, Emisividad, Análisis

Citation: CARDENAS-SANCHEZ, Enrique, DELGADILLO-PARTIDA, Jorge, RAMOS-PONCE, Manuel and RIOS-HERNANDEZ, Juan. Preliminary study of thermography applied to diagnosed faults in Diesel Engine and network rack. Journal of Computational Technologies. 2023. 7-19: 29-36

* Author Correspondence: (e-mail: enrique-cardenas@utmzo.onmicrosoft.com)
† Researcher contributing as first author.

Introduction

Due to the increasing demand for thermography devices in the industrial sector for industrial equipment monitoring and preventive maintenance, the production of these devices has been encouraged, with technological improvements in the most recent models. Due to their designs, functions and dimensions, they offer a diversity of applications in industry using thermal imaging, mainly for efficiency measurement, diagnosis, preventive inspections of failures in industry (Rao, 1998; Shepard, 1997; Bagavathiappan *et al*, 2013; Khamisan, *et. al*., 2018; Glowacz, 2021; Javed *et al*., 2022; Nakaguchi, & Ahamed, 2022; De La Cruz, 2023;Usai *et al*., 2023; Vásquez *et al*, 2023; Xu *et al*., 2023).

Heat on a regular basis is often an early symptom of damage or failure in Electrical and Mechanical Systems (EMS), making effective monitoring within preventive maintenance programmes highly relevant (Khamisan, et al., 2018). EMS is defined as the set of all the parts that make up a piece of equipment, including the mechanical part (where motion and friction occurs, such as in a diesel engine, turbine rotor, etc.) and the electrical part. Monitoring the performance of EMS with devices such as a thermal imaging camera reduces the likelihood of downtime due to EMS failures, reducing repair and maintenance costs, and extending the lifetime of assets.

On the other hand, Predictive Maintenance uses the analysis of thermographic data to identify operational anomalies and potential equipment defects, allowing timely repairs to be made before failures occur. For example, the industry can monitor various indicators, such as the decrease in rotational speed of an element caused by wear, as well as the lubrication or temperature reached by the system due to constant friction. On the other hand, using technology-based monitoring and the Internet of Things (IoT).

Corrective maintenance involves identifying, isolating and rectifying a fault so that the broken equipment or system can be restored to an operational condition. Thermography facilitates this process by providing visual evidence of the problem area.

For example, an infrared camera can identify electrical connection or component problems, such as misalignment, steam/water leaks, bent shafts, moisture, among others. This allows immediate corrective action to be taken, which positively impacts the indicators of time and resources spent on troubleshooting.

Microbolometer Sensor Rationale

The microbolometer sensor is an essential component in thermal imaging cameras. It functions as a radiation detector in the infrared spectrum of any radiating object, i.e. when its temperature is above absolute 0 on the Kelvin scale. The emitted radiation is converted into an electrical signal, which is then converted into an output image.

To develop the thermal image, the sensor has a number of microsensors. Each of them detects a corresponding value of the radiation emitted by the object to be studied. This set of information is displayed on a screen as an image composed of the same pixels that make up the sensor. Therefore, the higher the number of pixels in a device, the better the resolution and, therefore, the lower the degree of accumulated error in the measurement.

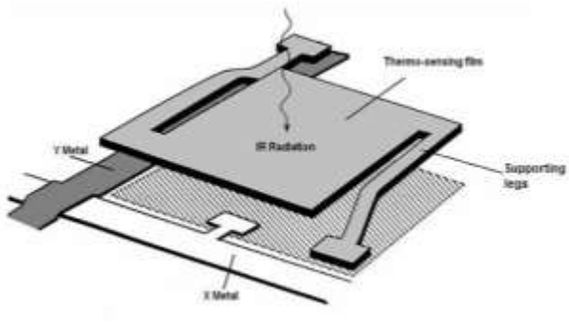

Figure 1 Example of the functioning of a microbolometer sensor and its parts
Image from Blanco-Mora (2013)

Following the principle of the photoelectric effect explained in 1905 and for which Albert Einstein was distinguished as Nobel Prize winner. Einstein explained mathematically how the energy of an electromagnetic wave collides with the electrons of some element; as an example, Vanadium or Silicon-Germanium (Blanco-Mora, 2013); see illustration in figure 1. Then, the radiative source when hitting the sensor emits an electrical signal later transformed into an image, as explained above.

ISSN 2523-6814

On the other hand, Wien's law explains the relationship between temperature and the length of the electromagnetic wave (Cardenas-Sanchez, 2013).

This law is expressed as:

$$\lambda_{max} * T = b \quad (1)$$

Where λ_{max} is the value of the maximum length of all total radiation emitted by the object. The value of b is equal to 2897.5 μmK. Wien's law is derived from Planck's radiation equation.

Thermal cameras equipped with microbolometer sensors cover wavelengths from 7 to 14 micrometres. As mentioned above, these chambers do not require special cooling systems, which makes them more affordable and smaller in size. They are therefore practical for field applications (Cárdenas-Sánchez *et al*, 2013).

The importance of emissivity on material diversity

It should be considered that these sensors do not measure the absolute temperature of objects; their operation is based on the measurement of the thermal emissivity (ε) of the incandescent object located at a specific distance (d) and emitting radiation in a range of frequencies with an emitting power E(λ, T), which depends on both frequency and temperature. To calculate the emissive power of any object at a given temperature and wavelength range, the Planck spectral emissive potential function is used, which describes how spectral radiation is emitted from a body at a given temperature, expressed in units of watts per cubic metre (W/m^3).

Emissivity, on the other hand, is a property of all materials and describes their ability to emit thermal radiation. It is expressed as a number between 0 and 1. In general, it represents the efficiency with which a material emits radiant energy in the form of heat at the infrared frequency. The emissivity of a material influences the amount of infrared (IR) radiation it emits when heated.

The emissivity of materials varies according to their petrological components. For example, materials that are good emitters of thermal radiation are close to 1, such as oxidised metals, asphalt, some volcanic rocks, etc. Classically, in physics, a material that emits and receives all radiation with an emissivity of 1 is known as blackbody radiation, see table 1.

Figure 2 shows an example of a thermal image capture to observe the variation of cooling. We can also observe the emissivity of this reflected on the table. The rate is this is polished so the emissivity is very low (less than 0.3), according to table 2 (Cardenas-Sanchez, 2013). On the other hand, note that with this equipment and software we can monitor the maximum temperature (indicated in the coffee rate) and minimum (indicated by the software in the lower left corner) to give sequence to the phenomenon. In this case it is a test example.

Material	Emissivity Range
Polished aluminium	0.05 – 0.10
Oxidised aluminium	0.07 – 0.95
Glass	0.80 – 0.95
Wood	0.90 – 0.95
Plastic	0.85 – 0.95
Cement	0.90 – 0.95
Volcanic rocks	0.95 – 0.98

Table 1 Emissivity range of some common materials *(Bagavathiappan, 2013 Harris, 2013: pp74)*

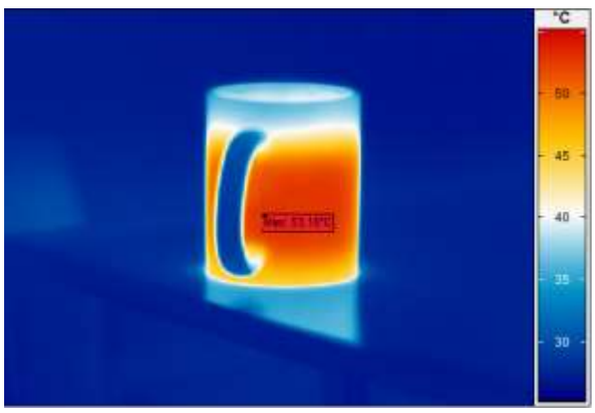

Figure 1 Example of emissivity measured on a coffee cup. Observe how it reflects the thermal radiation on the table on which it is placed. This radiation, if it were excessive, would explain why objects transmit part of the heat to their surroundings until thermal equilibrium is reached. Own image captured in the lab using Irbis 3 software

The emissivity value used for our experiments varies depending on the EMS being analysed.

ISSN 2523-6814

Tools, materials and software

Due to cost reductions in the thermographic industry and the incorporation of new technologies, such as the microbolometer sensor, the prices of thermographic equipment have decreased significantly in recent years. An example of this is the microbolometer sensor, which is cheaper compared to the old, expensive sensors that required specialised thermoelectric cooling systems.

Furthermore, in the Latin American context, there are security and licensing restrictions that limit the acquisition of thermographic equipment, especially with regard to data transmission, which is restricted to a maximum speed of 9 Hz. This limitation is not always fully understood by the various importers. However, it should be noted that the technological restriction on the data rate could be related to its exclusive use in the military industry in the North American and EU markets. This should be taken into consideration if you wish to purchase such equipment.

Team	Brand and other features
InfraTech thermal camera model VarioCam.	Microbolometer type sensor with a range of -40 to 1200 oC and a spectral range of 7.5 to 13 µm. Imaging resolution 640×480, viewing angle 1×30mm (30×23o).
Irbis 3 software	The software used for temperature analysis is Irbis version 3.0.
Lenovo Legion Laptop for information processing	Intel i7 9gen, with integrated GPU (not required for processing), and Windows 11 Home.
SD card	For capturing images on the thermal camera with standard 2Gb memory capacity.
Test engine	Diesel engine 6 cylinders in line, turbo charged, Perkins brand model T 6.3544, 150 HP
Panduit 48 Port Patch Panel	Part of the module 1 network rack.

Table 2 Materials used for our experimental tests.

Experimental Method

The methodology to be used in the experiment is divided into four key stages for the evaluation of the thermal condition of a diesel engine and a computer network rack:

The calibration of the thermal emissivity will be performed separately considering the specific material of the engine and the network rack, as they are objects with different materials from each other. This calibration is essential to ensure accurate and reliable measurements of the surface temperatures of the engine and the rack. Standard references shall be used and the emissivity of the equipment shall be adjusted according to the material characteristics.

Data capture:

Data capture shall be performed while the test engine is running. During a continuous period of 30 minutes, thermal data will be collected using a thermal camera at a rate of 20 images per minute. It should be noted that the engine has previously recognised and diagnosed faults, which allows the identification of specific problem areas. This process will be repeated to minimise possible measurement errors and ensure consistency of results, Figure 2.

In the case of the network rack, especially the 48-port Patch panel device, it is located at the Technological University of Manzanillo. The rack, Figure 3, the device, allows the connection of 48 nodes simultaneously, and it is in constant operation 24 hours a day in climate controlled conditions. The air conditioning indicates a temperature of approximately 24 degrees Celsius on average. However, for the measurement, we have captured data during 2 different stages of the day. The first stage was at 9 o'clock in the morning, as this is the peak time for users to connect. Finally, the second stage was set at 2 p.m., as this is the time when users are least likely to be online. For this experiment, sampling was carried out at a capture rate of 20 seconds per image for 30 minutes.

Using the Irbis 3 software of the InfraTech thermal camera, the captured thermal images will be analysed in real time. The software will identify and highlight areas with thermal anomalies that may be related to possible engine damage. For the measurement of the images, in addition to detecting the anomalies directly, test points and sampling areas will be established on the images in time sequences. The test points are fixed points of a pixel of the image where the temporal evolution of the cooling or heating process of the thermal anomalies can be appreciated.

ISSN 2523-6814

In the case of sampling areas, they are predefined areas comprising several pixels that completely cover the anomaly. However, unlike point sampling, sampling areas indicate the maximum, minimum and average temperature of the observed area.

Once the thermal anomalies have been identified, it shall be determined whether they correspond to damaged or problematic parts of the diesel engine. The affected areas will be compared with the previous fault diagnosis to establish a correlation between the anomalous temperatures and the specific parts of the engine that require attention.

This comprehensive methodology will effectively assess the thermal condition of the diesel engine and determine if the detected thermal anomalies are related to the damaged areas, thus facilitating the diagnosis and repair process in the maintenance workshop.

Figure 2 Front view of the Network Rack used for our experiment

Figure 3 Diesel engine used for our experiment, Perkins model T 6.3544, 150 HP

Results and discussion

As mentioned in the methodology, the data collection was carried out in a similar way in both experiments. The difference between the two experiments was the thermal emissivity value.

However, the Network Rack has several elements of different materials, from plastic, in the connection cables, to elements combined with painted aluminium, mainly in the 48-port Patch, figure 3. We performed 3 tests with different emissivity values, as shown in table 3. According to the responsible for the maintenance and management of the network system of the Technological University of Manzanillo, the network centre presents a significant deterioration in that element. On the contrary, in the same rack is located a 24-node Patch whose temperatures are below 35 degrees, compared to the more than 50 degrees registered by the 48-node Patch, figure 6. In this sense, we observe that the lower the emissivity, the higher the temperature value observed. Further analysis is still required, this time using another sensor for comparison.

According to our analysis, the 48-node patch has a higher heating than normal mainly during peak hours, that is during the early morning hours, when several users are connected simultaneously, figure 7. In the case of the cooling rate, the sampling areas (C4 and C5) have a lower decay compared to a specific point in the area (P1, P2 and P3), this may be due to the stability of the support used. It is therefore advisable to fix the thermal camera on a solid base, in case a similar analysis is desired.

ISSN 2523-6814

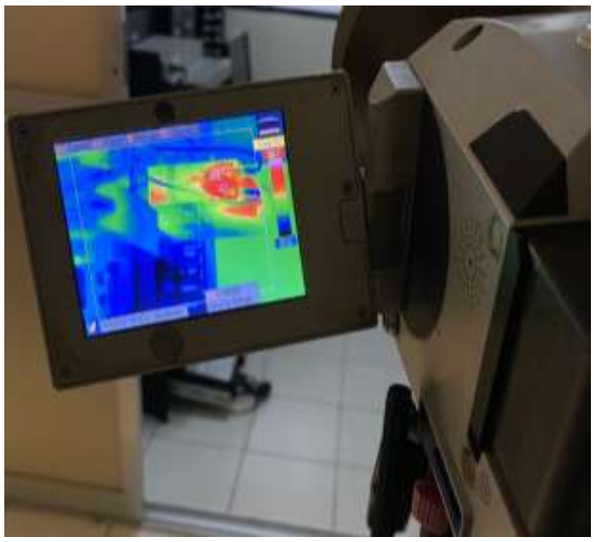

Figure 4 Photograph of the thermography equipment capturing data at a distance of approximately 1.5m from the network centre. This image clearly shows the thermal anomaly mainly in the 48-node Patch module

	Test 1	Test 2	Test 3
Experiment start time	10:19 a.m.	2:50 p.m.	11:17 a.m.
Emissivity	0.95	0.9	0.8
Laboratory temperature	24° C	24° C	24°C
Initial module temperature	40° C	46° C	51° C
Ambient temperature	33° C	32° C	31° C
Relative humidity	69%	68%	71%
Module end temperature	41° C	48° C	49.5° C

Table 3 Table of data for the three tests performed in the Network Rack indicating date, start time, temperature of the cooling system.

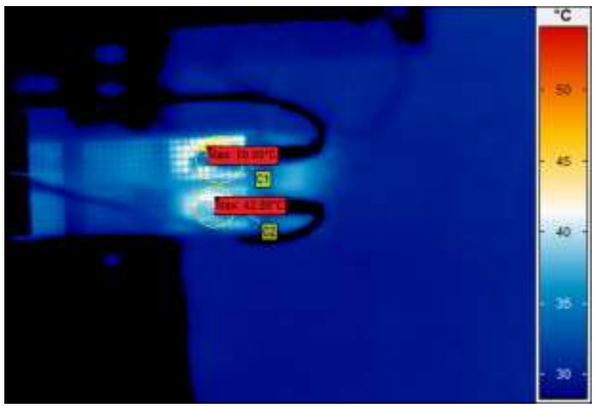

Figure 5 Analysis of the thermal anomalies detailing the high temperatures recorded. The image corresponds to the third experiment, table 3. On the other hand, the average temperature is below 30 degrees Celsius, the highest values can range up to 52 degrees Celsius.

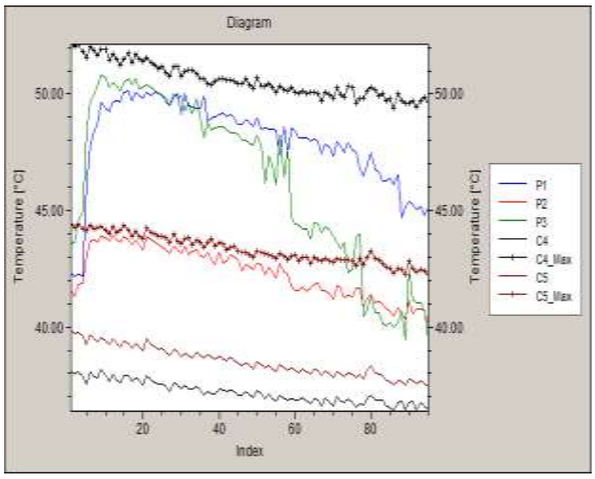

Figure 6 Anomaly analysis for the network rack using 90 images captured every 20 seconds. Note that some sampling points (P1, P2, and P3) decay with higher speed, these are sampling points (the size of the size of 1 pixel). On the other hand, the sampling areas (C4 and C5) show a curve with an almost constant mean value, because it considers the average value of the whole area.

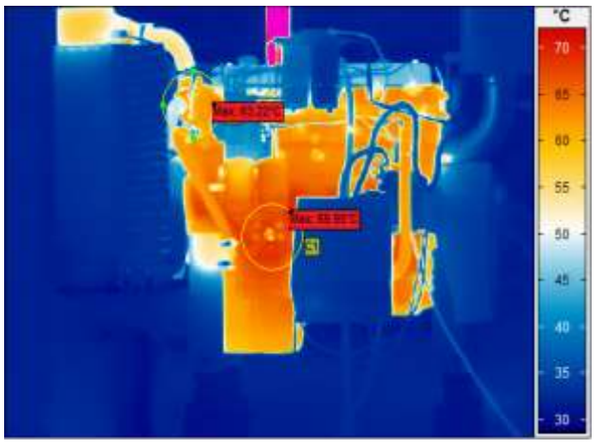

Figure 7 Test T-engine for our analysis with known faults. The image shows sampling areas with circle geometry listed as C1, and C2 respectively

On the emissivity in the engine study, we chose the value of 0.8 fixed for the two tests we did, this choice was due to the rough carbon steel components that make up the main engine casing. Therefore, in general terms the correct analysis performance is in the range of 0.8 to 0.9 in reality. We should continue to perform similar experiments in the future testing emissivity values in this range.

In figure 8, on the combustion engine, it can be seen that there is no coolant circulation from the monoblock to the radiator and temperatures of 35 Celsius. On the other hand, for our experiment we chose that the cooling system has a low coolant level as an induced failure.

ISSN 2523-6814

As can be seen in the figure, the equipment has an oil cooler that dissipates the temperature given off by the engine, which can be clearly seen in Circle 1, which is also where the largest temperature range recorded is observed, in addition to the exhaust system. In addition, there is a fault in its thermostats due to the fact that they do not open to the correct temperature (circle 2). Maintaining equipment in this condition could cause catastrophic failures for bearings, connecting rods, crankshaft and monoblock, among others. With the support of thermography we can anticipate possible failure of internal elements that make up an internal combustion engine and avoid corrective maintenance repair costs.

We have also carried out a temporal analysis of the data for our experiment. Although we performed 3 tests under similar conditions; temperature, emissivity and sampling time. However, we observed slight changes over time. Figure 9 shows the time series analysis of the captured images. In total there were 90 images captured at a rate of 3 per minute, or every 20 seconds. Note in figure 9, that the analysis of all the time series data, prior to engine shutdown, shows a higher growth rate over the oil cooler, as opposed to the cooling system, at C2.

On the other hand, the sudden changes in temperature around 30 seconds are due to changes in the thermal chamber, as it was not bolted to the base.

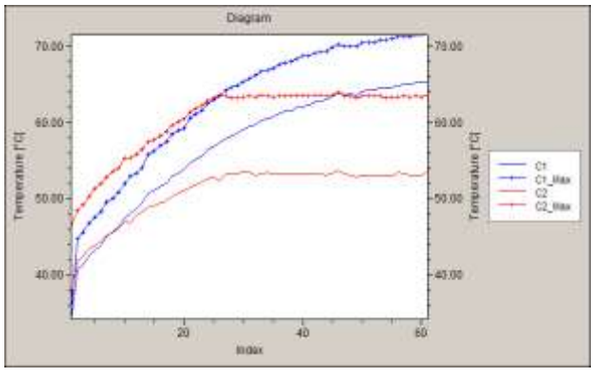

Figure 9 The figure shows the maximum, minimum and average values of circles 1, and 2 respectively in figure 8. Circle 1, above the oil cooler, also shows higher temperature values than the rest of its components

Conclusions

Thermography applied in SEM, such as those described in this article, allowed us to monitor the vulnerable regions in each of the systems analysed, mainly in the emissivity study. However, further studies and comparisons with other sensors are still needed. On the other hand, the preliminary analysis shows interesting results by highlighting high temperatures in areas such as the cooling system of the combustion engine. As an area of opportunity, in subsequent studies, the same engine will be studied again in order to confirm the predictions in order to subsequently carry out repairs, and to observe the difference between the two conditions of the engine under study. The emissivity at 0.8 reflects an adequate score, validated by a sensor device belonging to the same engine, with values around 85 degrees Celsius.

Similarly, in the network rack, the fact of previously knowing the failure on the 48-node patch allows us to have a maximum temperature threshold when it is required during the hours of highest traffic connection service and its comparison during the hours of low demand, as shown in the graph in figure 7. In this sense, this experiment also allowed us to know the effective emissivity ranges for the analysis. In our investigation, the 24-node patch did not show temperature values as high as the 48-node patch. This is logical because the 24-node patch is not faulty and is working normally.

We are aware of the failure of both the patch and the analysed engine. Nevertheless, these experiments have allowed us to build up a database that will grow as we conduct further experiments. With this data, in the future we will be able to define the predominant variables (essential features or characteristics that distinguish the neural network) that will feed the neural network as input data. This is an area of opportunity to generate an automated fault analysis system for similar systems. Below, you can find our database at the following GitHub link exclusively for educational use.

ISSN 2523-6814

Acknowledgements and funding

Special thanks to Dr. Nick Varley of the University of Colima for his technological contribution of the instrument for this research project. In addition, to MTI. Bonni Burst Beltrán, director of the School Administration area, and the team of collaborators in the Systems area for allowing us to use their facilities for our project. Last but not least, to the students of the Universidad Tecnológica de Manzanillo from the Industrial Maintenance Engineering area for their contribution to our research.

References

Bagavathiappan, S., Lahiri, B. B., Saravanan, T., Philip, J., & Jayakumar, T. (2013). Infrared thermography for condition monitoring–A review. Infrared Physics & Technology, 60, 35-55. https://doi.org/10.1016/j.infrared.2013.03.006

Blanco-Mora, D. A. (2013), Diseño de circuitos integrados de lectura para microbolómetro, Tesis de Maestría INAOE. Fuente:https://inaoe.repositorioinstitucional.mx/jspui/bitstream/1009/255/1/BlancoMDA.pdf

Cárdenas-Sánchez, E., (2013), Modelo de enfriamiento de clastos volcánicos para la estimación de la energía térmica liberada por una explosión vulcaniana o Stromboliana, Tesis UNAM,http://132.248.9.195/ptd2013/enero/0687090/Index.html

Glowacz, A. (2021). Fault diagnosis of electric impact drills using thermal imaging. Measurement, 171, 108815.
Harris, A. (2013). Thermal remote sensing of active volcanoes: a user's manual. Cambridge university press. https://doi.org/10.1017/CBO9781139029346

Javed, M. R., Shabbir, Z., Asghar, F., Amjad, W., Mahmood, F., Khan, M. O., ... & Haider, Z. M. (2022). An Efficient Fault Detection Method for Induction Motors Using Thermal Imaging and Machine Vision. Sustainability, 14(15), 9060. https://doi.org/10.3390/su14159060

Khamisan, N., Ghazali, K. H., Almisreb, A., & Muhammad Zin, A. H. (2018). Histogram-based of Healthy and Unhealthy Bearing Monitoring in Induction Motor by Using Thermal Camera. Journal of Telecommunication, Electronic and Computer Engineering (JTEC), 10(1-9), 31–35. Retrieved from https://jtec.utem.edu.my/jtec/article/view/3867

Nakaguchi, V. M., & Ahamed, T. (2022). Fast and Non-Destructive Quail Egg Freshness Assessment Using a Thermal Camera and Deep Learning-Based Air Cell Detection Algorithms for the Revalidation of the Expiration Date of Eggs. Sensors, 22(20), 7703. https://doi.org/10.3390/s22207703

Rao, B.K.N. (1998). Condition monitoring and the integrity of industrial systems. In: Davies, A. (eds) Handbook of Condition Monitoring. Springer, Dordrecht. https://doi.org/10.1007/978-94-011-4924-2_1

Shepard, S.M. (1997), "Introduction to active thermography for non-destructive evaluation", Anti-Corrosion Methods and Materials, Vol. 44 No. 4, pp. 236-239. https://doi.org/10.1108/00035599710183199

Xu, B., Sun, B., Cui, L., Chen, J., Chen, X., Li, X., ... y Xue, Y. (2023). Evaluation of the star anise extract as a natural cold flow improver for enhancing the cold flow properties of diesel fuel. Renewable energy, 215, 119028. https://doi.org/10.1016/j.renene.2023.119028

Usai, V., Marelli, S. y Cordalonga, C. (2023). Heat Transfer Correction Model for Turbocharger Compressor Performance Maps, SAE Technical Paper 2023-01-0179, 2023, https://doi.org/10.4271/2023-01-0179.

De La Cruz, J., Gómez-Luna, E., Ali, M., Vásquez, JC y Guerrero, JM (2023). Fault Location for Distribution Smart Grids: Literature Overview, Challenges, Solutions, and Future Trends. *Energies*, 16 (5), 2280. https://doi.org/10.3390/en16052280

ISSN 2523-6814